



New excited state intramolecular proton transfer dyes based on naphthalenediimides (NDI) and its population of triplet excited state

Jie Ma^{*}, Jinlong Li, Rui Yang, Weijian Xue, Qingxia Wang, Shenmiao Li

Heilongjiang Provincial Key Laboratory of Catalytic Synthesis for Fine Chemicals, College of Chemistry and Chemical Engineering, Qiqihar University, Qiqihar, 161006, PR China

ARTICLE INFO

Keywords:

Naphthalenediimides
2-(2-Hydroxyphenyl)Benzothiazole
Excited state intramolecular proton transfer
Triplet excited state

ABSTRACT

The dyes of Naphthalenediimides (NDI) conjugated and non-conjugated with 2-(2-Hydroxyphenyl)Benzothiazole (N-1~N-5) were prepared. The compounds showed dramatically red-shifted UV-vis absorption (483–611 nm) and emission (538–635 nm) compared with traditional ESIPT compound (HBT). Among them, N-1 shows obvious dual emission at 538 nm (enol form), 682 nm (keto form) in PhCH₃ and large Stokes shift (up to 144 nm), which is one of the evidence for the characteristics of ESIPT. Time-resolved transient absorption demonstrated triplet excited states were populated upon photoexcitation for all the compounds. Especially for N-3 and N-4, the life time of triplet excited states (τ_T) are 48.0 μ s and 148.5 μ s, respectively. The lifetime of triplet excited state were also observed in N-1 ($\tau_T = 72.0 \mu$ s) and N-2 ($\tau_T = 121.1 \mu$ s). The population of triplet excited states of all the compounds were testified by photooxidation for 1, 3-diphenylisobenzofuran. N-3 and N-4 exhibit much efficient photooxidative ability than N-1, N-2 and N-5.

1. Introduction

Excited state intramolecular proton transfer, as a unique photo-physical phenomenon, has been widely used in the areas of molecular probes [1–5], luminescent materials [6–16], and molecular logic gates [17,18], etc. Compared with normal fluorophores, ESIPT chromophores possess large Stokes shift (up to 200 nm) and low fluorescence quantum yields. Traditional ESIPT chromophores, such as 2-(2-hydroxyphenyl) benzothiazole (HBT) and 2-(2-hydroxyphenyl) benzoxazole HBO [19], which show weak absorption in visible range. This property limits their applications in the area of luminescent molecular probes and luminescent materials, etc. The effective method is to broaden the size of π -conjugation framework of a chromophore. However, such molecule of HBT and HBO with large extension in n -conjugation structure is seldom reported [20–22].

On the other hand, naphthalenediimides (NDI) is a well-known fluorophore which shows the absorption and emission in visible spectral region and high photostability. NDI derivatives have been applied intensively as fluorescent molecular probes [23–29] and as a scaffold in molecular arrays [30–37]. Especially amino-substituent structures, give strong visible absorption and emission in red area [33,35,38–40]. Up to now, NDI has never been used to combine with ESIPT chromophore.

It is worth noting that triplet excited state will be populated by photoexcitation of ESIPT chromophore [19,41,42]. However, ISC is difficult for the absence of heavy atom molecules, because $S_1 \rightarrow T_1$ is forbidden transition [43–45]. We notice triplet excited states origin from ESIPT dyes maybe provide a new route for heavy-atom free photosensitizers. Concerning the aforementioned challenges, herein we prepared a series of compounds with moieties of HBT and NDI (N-1~N-5) to study ESIPT process and the population of triplet excited state.

2. Experimental

2.1. Analytical measurements and reagents

NMR spectra were recorded by a Bruker 600 MHz spectrometer with CDCl₃ as solvent. High-resolution mass spectra (HRMS) were measured in a MALDI-HR MS system (U.K.). The absorption spectra were recorded on UV2550 UV-vis spectrophotometer (Shimadzu, Japan) and Agilent 8453 UV-vis near-IR spectrophotometer. Fluorescence spectra were measured on a RF5301 PC spectrofluorometer (Shimadzu, Japan). Fluorescence lifetimes were recorded with OB920 luminescence lifetime spectrometer (Edinburgh Instruments, U.K.).

The reagents were analytically pure and the solvents were dried and

^{*} Corresponding author.

E-mail address: majie722@126.com (J. Ma).

<https://doi.org/10.1016/j.dyepig.2021.109225>

Received 29 August 2020; Received in revised form 2 February 2021; Accepted 4 February 2021

Available online 14 February 2021

0143-7208/© 2021 Elsevier Ltd. All rights reserved.

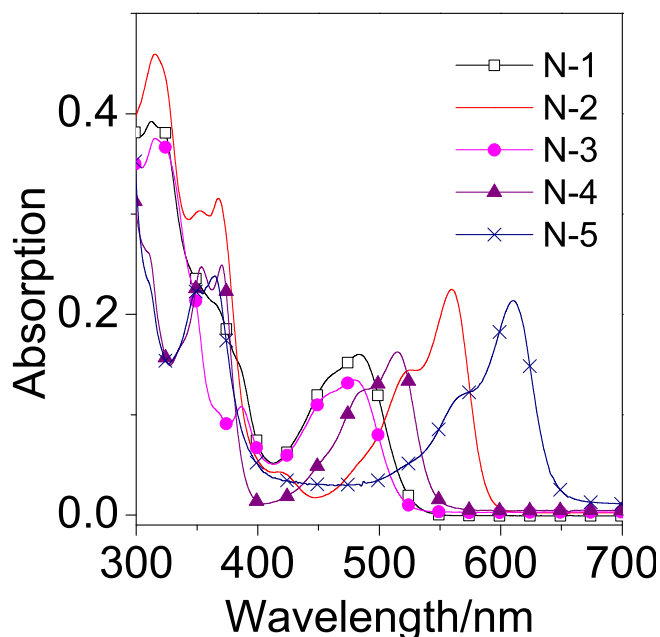


Fig. 1. UV-vis absorption of N-1~N-5. $c = 1.0 \times 10^{-5}$ M in PhCH₃, 20 °C.

(t, 2H, $J = 7.8$ Hz), 2.03–1.93 (m, 2H), 1.82–1.78 (m, 1H), 1.55–1.30 (m, 24H), 1.01–0.88 (m, 18H). ¹³C NMR (150 MHz, CDCl₃): 167.91, 165.78, 162.36, 162.08, 161.48, 158.12, 151.51, 150.96, 136.41, 135.96, 132.12, 131.85, 126.89, 126.24, 125.23, 124.35, 121.89, 121.64, 121.05, 120.12, 119.34, 117.77, 116.24, 114.03, 99.44, 97.05, 88.60, 46.00, 44.04, 43.31, 38.79, 37.39, 37.25, 30.65, 30.18, 29.17, 28.33, 28.14, 24.03, 23.63, 23.53, 22.67, 22.61, 22.52, 13.55, 10.45, 10.22. MALDI-HRMS: m/z calcd for [C₃₈H₅₄BrN₃O₄ + H]⁺ 867.4514; found: 867.4525.

2.2.3. Synthesis of compound N-3

N-3 was obtained according to the following the procedure similar to that of N-1, except **9** (30 mg, 0.13 mmol) was used instead of **8**. Orange solid (35 mg), yield: 42.4% [1]. ¹H NMR (600 MHz, CDCl₃): δ 8.92 (d, 1H, $J = 2.1$ Hz), 8.86 (s, 1H), 8.76 (d, 1H, $J = 7.6$ Hz), 8.69 (d, 1H, $J = 7.6$ Hz), 8.14 (d, 1H, $J = 8.1$ Hz), 7.97 (d, 1H, $J = 7.8$ Hz), 7.85 (m, 1H), 7.85 (m, 1H), 7.53 (t, 1H, $J = 7.2$ Hz), 7.41 (t, 1H, $J = 7.2$ Hz), 7.11 (d, 1H, $J = 8.6$ Hz), 4.29 (t, 2H, $J = 6.5$ Hz), 4.24–4.09 (m, 4H), 2.08–2.02 (m, 3H), 1.96–1.91 (m, 1H), 1.71–1.64 (m, 2H), 1.43–1.31 (m, 16H), 1.08 (t, 3H, $J = 7.3$ Hz), 0.99–0.88 (m, 12H). ¹³C NMR (150 MHz, CDCl₃): 162.00, 162.80, 162.58, 161.65, 161.61, 161.24, 161.18, 157.47, 151.89, 136.84, 136.11, 135.91, 133.75, 130.91, 130.03, 127.70, 127.38, 126.05, 125.30, 125.13, 124.95, 124.83, 123.04, 122.27, 122.20, 121.22, 115.20, 112.22, 111.76, 102.71, 89.79, 69.43, 44.53, 37.89, 31.18, 30.72, 28.64, 24.04, 23.06, 19.54, 14.16, 14.12, 13.94, 10.67. MALDI-HRMS: m/z calcd for [C₄₉H₅₃N₃O₅S-H]⁻ 795.3700; found: 795.3713.

2.2.4. Synthesis of compound N-4

Under Ar atmosphere, **6** (50.0 mg, 0.085 mmol) and **8** (30.0 mg, 0.12 mmol) were dissolved in the mixed solvent (14 mL, CHCl₃:EtOH: H₂O = 12:1:1, v/v). Then CuSO₄·5H₂O (4.5 mg) and sodium ascorbate (7.2 mg) was added respectively. The resulting mixture was stirred at 35 °C for 24 h. Then the reaction mixture was washed with brine and extracted with CH₂Cl₂. Organic layer was dried over anhydrous Na₂SO₄ and evaporated under reduced pressure. The crude product was purified by column chromatography (silica gel, CH₂Cl₂: CH₃OH = 100 : 1, v/v) to give red solid. Yield: 48 mg, 67.3%. ¹H NMR (400 MHz, CDCl₃): δ 12.71 (s, 1H), 10.22 (t, 1H, $J = 7.8$ Hz), 8.64 (d, 1H, $J = 7.8$ Hz), 8.35 (d, 1H, $J = 7.8$ Hz), 8.20 (d, 1H, $J = 1.9$ Hz), 8.17 (s, 1H), 8.02 (d, 1H, $J = 8.1$ Hz),

7.94 (d, 1H, $J = 7.9$ Hz), 7.84 (s, 1H), 7.74 (d, 1H, $J = 2.0$ Hz), 7.53 (t, 1H, $J = 7.2$ Hz), 7.44 (t, 1H, $J = 7.2$ Hz), 7.15 (d, 1H, $J = 7.5$ Hz), 4.66 (t, 2H, $J = 6.6$ Hz), 4.15–4.04 (m, 4H), 3.74–3.71 (m, 2H), 2.57–2.53 (m, 2H), 1.95–1.86 (m, 2H), 1.38–1.28 (m, 16H), 0.93–0.86 (m, 12H). ¹³C NMR (150 MHz, CDCl₃): 168.84, 166.46, 163.53, 163.07, 157.95, 151.93, 151.58, 147.12, 132.57, 131.38, 130.07, 129.16, 127.87, 126.81, 126.03, 125.73, 125.28, 124.82, 123.50, 122.19, 121.55, 119.39, 119.34, 119.03, 118.34, 116.86, 100.37, 47.77, 44.49, 43.91, 40.12, 37.78, 30.72, 29.86, 28.68, 28.64, 24.03, 23.04, 14.11, 10.69. MALDI-HRMS: m/z calcd for [C₄₈H₅₃N₇O₅S-H]⁻ 839.3823; found: 839.3814.

2.2.5. Synthesis of compound N-5

Under Ar atmosphere, **7** (43.0 mg, 0.06 mmol) and **8** (15.0 mg, 0.06 mmol) were dissolved in the mixed solvent (14 mL, CHCl₃: EtOH: H₂O = 12 : 1 : 1, v/v). Then CuSO₄·5H₂O (4.5 mg) and sodium ascorbate (7.2 mg) was added respectively. The resulting mixture was stirred at 35 °C for 48 h. Then the reaction mixture was washed with brine and extracted with CH₂Cl₂. Organic layer was dried over anhydrous Na₂SO₄ and evaporated under reduced pressure. The crude product was purified by column chromatography (silica gel, CH₂Cl₂: CH₃OH = 100 : 1, v/v) to give purple solid. Yield: 50 mg, 86.2%. ¹H NMR (400 MHz, CDCl₃): δ 12.71 (s, 1H), 9.45–9.39 (m, 2H), 8.17 (s, 1H), 8.10 (s, 1H), 8.06 (s, 1H), 8.00 (d, 1H, $J = 8.1$ Hz), 7.92 (d, 1H, $J = 7.9$ Hz), 7.84 (s, 1H), 7.73 (d, 1H, $J = 8.2$ Hz), 7.52 (t, 1H, $J = 7.2$ Hz), 7.43 (t, 1H, $J = 7.3$ Hz), 7.13 (d, 1H, $J = 8.5$ Hz), 4.64 (t, 2H, $J = 6.6$ Hz), 4.11–4.05 (m, 4H), 3.64–3.60 (m, 2H), 3.36 (t, 1H, $J = 5.7$ Hz), 2.53–2.49 (m, 2H), 1.77–1.71 (m, 1H), 1.53–1.48 (m, 2H), 1.45–1.43 (m, 2H), 1.37–1.28 (m, 20H), 0.98–0.86 (m, 18H). ¹³C NMR (150 MHz, CDCl₃): 169.06, 169.03, 166.53, 166.30, 163.23, 163.17, 157.94, 151.66, 149.49, 148.42, 146.93, 132.68, 130.12, 126.73, 125.65, 125.56, 125.35, 122.34, 122.17, 121.57, 121.28, 120.85, 118.79, 118.33, 117.37, 116.92, 102.44, 101.35, 48.01, 46.36, 43.96, 40.01, 39.17, 37.85, 31.21, 30.78, 29.76, 28.85, 28.82, 28.70, 28.86, 24.56, 24.07, 23.13, 23.02, 14.12, 10.98, 10.63. MALDI-HRMS: m/z calcd for [C₅₆H₇₀N₈O₅S-H]⁻ 966.5184; found: 966.5174.

3. Results and discussion

3.1. Design and synthesis

We prepared the dyes (N-1 and N-2) of NDI conjugated with HBT by Pd (0) catalyzed Sonogashira coupling reaction. The acetylenic bond (C≡C) linker was introduced into the molecules. With introduction of alkylamino group into NDI core, N-2 was prepared to access larger absorption compared with N-1. In order to compare the difference of the conjugation and non-conjugation structures, we also prepared the dyads (N-4 and N-5) by click reaction catalyzed by Cu(0). The key procedure is that bromo-atom in NDI is substituted by 3-azidopropan-1-amine. All the compounds were obtained in moderate to satisfying yields. (see experimental section and ESI† for details). The synthetic route was described in Scheme 1.

3.2. Uv-vis absorption and fluorescence emission spectrums

The UV-Vis absorption spectra of the compounds (N-1~N-5) were studied (Fig. 1). The absorption band at about 300–320 nm is probably attributed to the enol-form of HBT moieties. The absorption maximums of all the compounds are not very sensitive to solvent polarity, which suggested proton transfer process doesn't occur in the ground state. N-1 gives the absorption maximum at 483 nm in toluene ($\epsilon = 16900$ M⁻¹cm⁻¹). Compared to N-1, stronger absorption band of N-2 shows dramatically red-shift ($\lambda_{\text{abs}} = 560$ nm, $\epsilon = 22500$ M⁻¹cm⁻¹) due to the substitution of alkylamino group [33].

By click reaction, the compounds of non-conjugation with HBT (N-4 and N-5) were also studied [46,47]. With introduction of one or two alkylamino groups, absorption bands of N-4 and N-5 move to 515 and

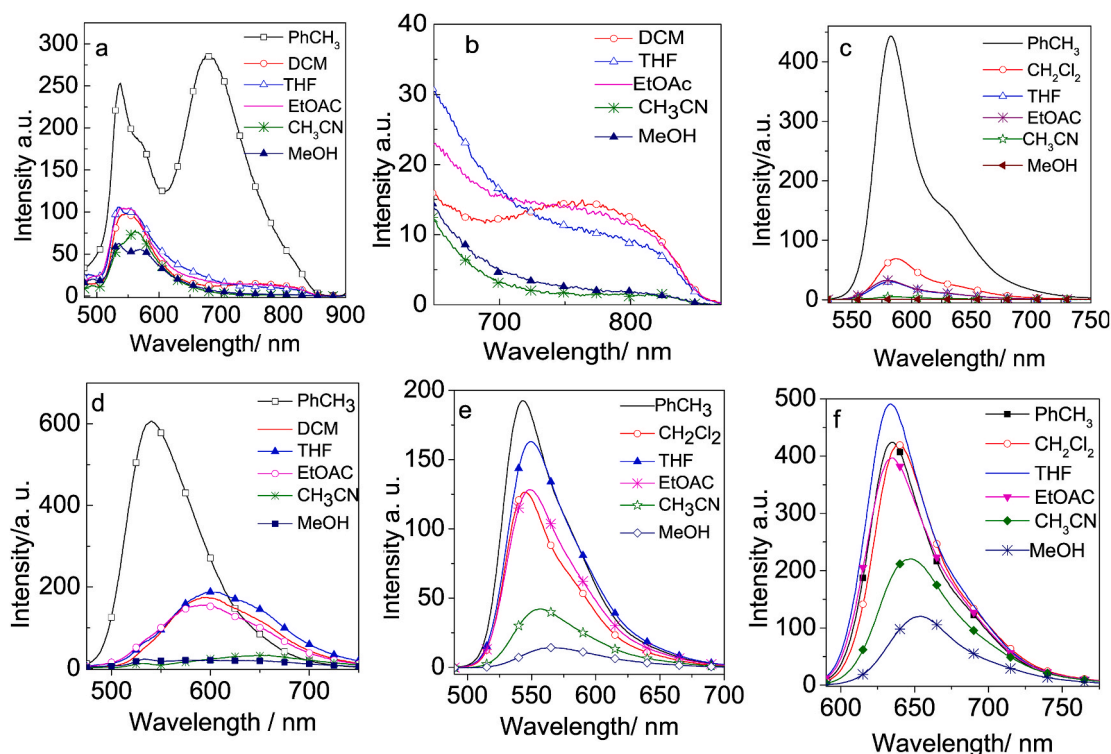


Fig. 2. Fluorescence emission spectra of (a) N-1 ($\lambda_{\text{ex}} = 460$ nm) (b) magnified emission spectrum of cis-keto isomer of N-1 (c) N-2 ($\lambda_{\text{ex}} = 520$ nm); (d) N-3 ($\lambda_{\text{ex}} = 460$ nm); (e) N-4 ($\lambda_{\text{ex}} = 480$ nm); (f) N-5 ($\lambda_{\text{ex}} = 580$ nm) in different solutions. $c = 1.0 \times 10^{-5}$ M, 20°C .

Table 1

Photophysical properties of N-1, N-2, N-3, N-4 and N-5^a.

Comp	solvent	λ_{abs}^b (nm)	ϵ^c ($\text{M}^{-1}\text{cm}^{-1}$)	λ_{em}^d (nm)	τ^e (ns)	Φ_{F}^i %	Φ_{Δ}^k %	τ_{T}^f (μs)	
								N ₂	air
N-1	PhCH ₃	483	16900	538	1.91	68.9	14.7	72.0	0.59
	DCM	474	17000	682	0.12	9.8			
	THF	466	16900	537	8.85	4.4			
	MeOH	463	14200	536	j	j		.g	.g
	PhCH ₃	560	22500	582	9.01	62.3	11.2	121.1	0.38
N-2	DCM	558	22300	587	2.02	8.4			
	THF	555	22300	582	j	3.9			
	MeOH	556	15400	.p	.p			.g	.g
N-3	PhCH ₃	479	13400	541	.p	.p	27.7	48.0	0.59
	DCM	469	16200	592	.p	.p			
	THF	463	16600	600	j	.p			
	MeOH	461	15500	.p	.p			.g	.g
N-4	PhCH ₃	515	16300	543	4.31	24.3	19.4	148.5	0.59
	DCM	516	12800	545	2.72	11.3			
	THF	513	13200	549	j	17.5			
	MeOH	517	11900	566	.p	.p		.g	.g
N-5	PhCH ₃	611	21400	635	9.72	26.2	.p	.g	.g
	DCM	611	20900	638	9.29	23.2			
	THF	606	21200	634	j	25.2			
	MeOH	617	14500	654	j	j		.g	.g

^a The excited wavelength for compound N-1, N-2, N-3, N-4 and N-5 were 460 nm, 520 nm, 460 nm, 480 nm and 580 nm respectively (1.0×10^{-5} M, 20°C).

^b Absorption wavelength.

^c Molar extinction coefficient.

^d Fluorescence emission wavelength.

^e Fluorescence lifetimes.

^f Triplet state lifetimes.

^g No signal.

^k Quantum yield of singlet oxygen ($^1\text{O}_2$), Ru(bpy)₃ as standard ($\Phi_{\Delta} = 0.57$ in CH₃CN, $\lambda_{\text{ex}} = 470$ nm for N-1 and N-3); with Rose Bengal (RB) as standard ($\Phi_{\Delta} = 0.80$ in MeOH, $\lambda_{\text{ex}} = 560$ nm for N-2) and with 2,6-diiodo-Bodipy as standard ($\Phi_{\Delta} = 0.83$ in CH₂Cl₂, $\lambda_{\text{ex}} = 515$ nm for N-4).

ⁱ Fluorescence quantum yields with compound 2,6-diiodo-Bodipy as the standard ($\Phi_{\text{F}} = 0.027$ in CH₃CN) for N-1, N-2, N-3 and N-4, with methylene blue as standard ($\Phi_{\text{F}} = 0.03$ in CH₃OH) for N-5. Not determined.

^p Weak signal.

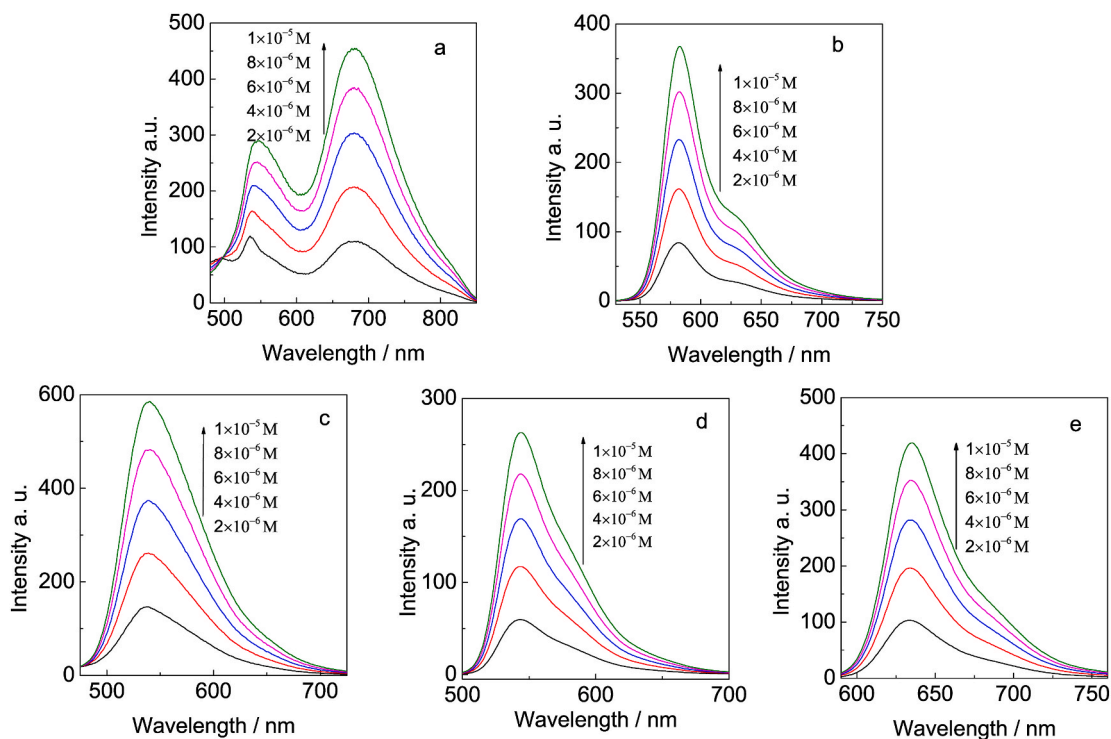


Fig. 3. Fluorescence emission spectra (a) N-1, (b) N-2, (c) N-3, (d) N-4 and (e) N-5 at the different concentration, in PhCH₃ at 20 °C.

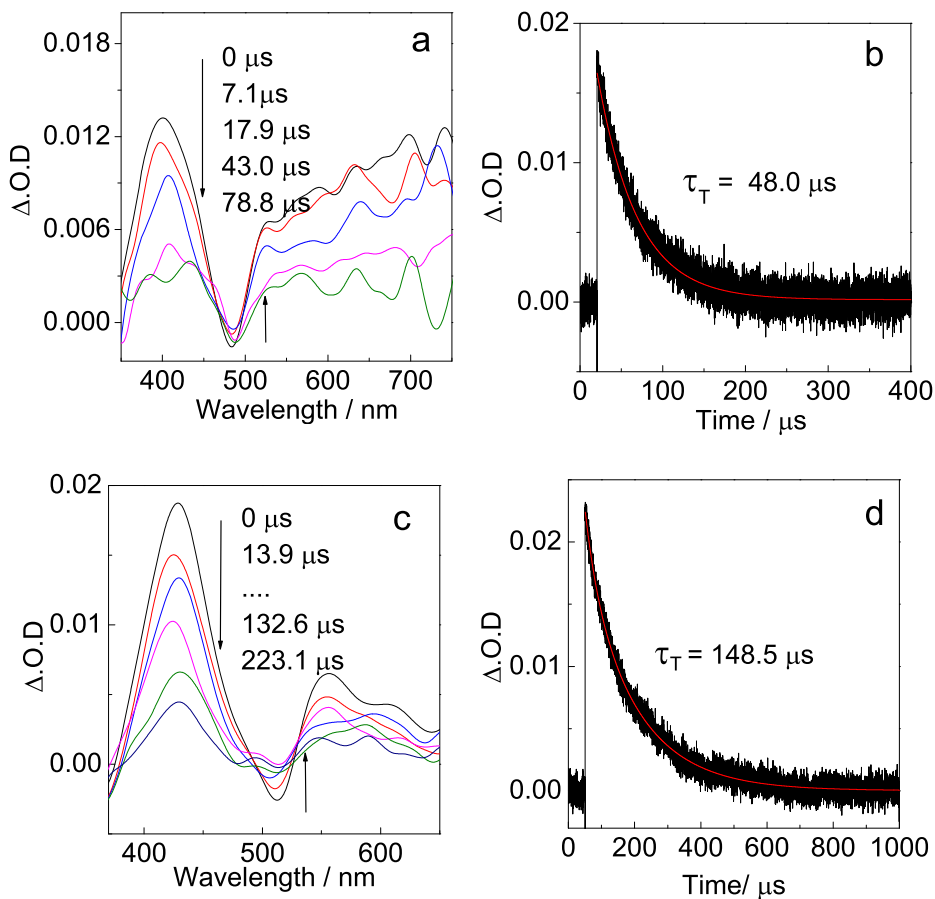


Fig. 4. Nanosecond time-resolved transient difference absorption of (a) N-3 ($\lambda_{ex} = 480$ nm) and (c) N-4 ($\lambda_{ex} = 515$ nm) after pulsed laser excitation. Decay trace of (b) N-3 at 400 nm and (d) N-4 at 430 nm in deaerated PhCH₃. $c = 2.0 \times 10^{-5}$ M, 20 °C.

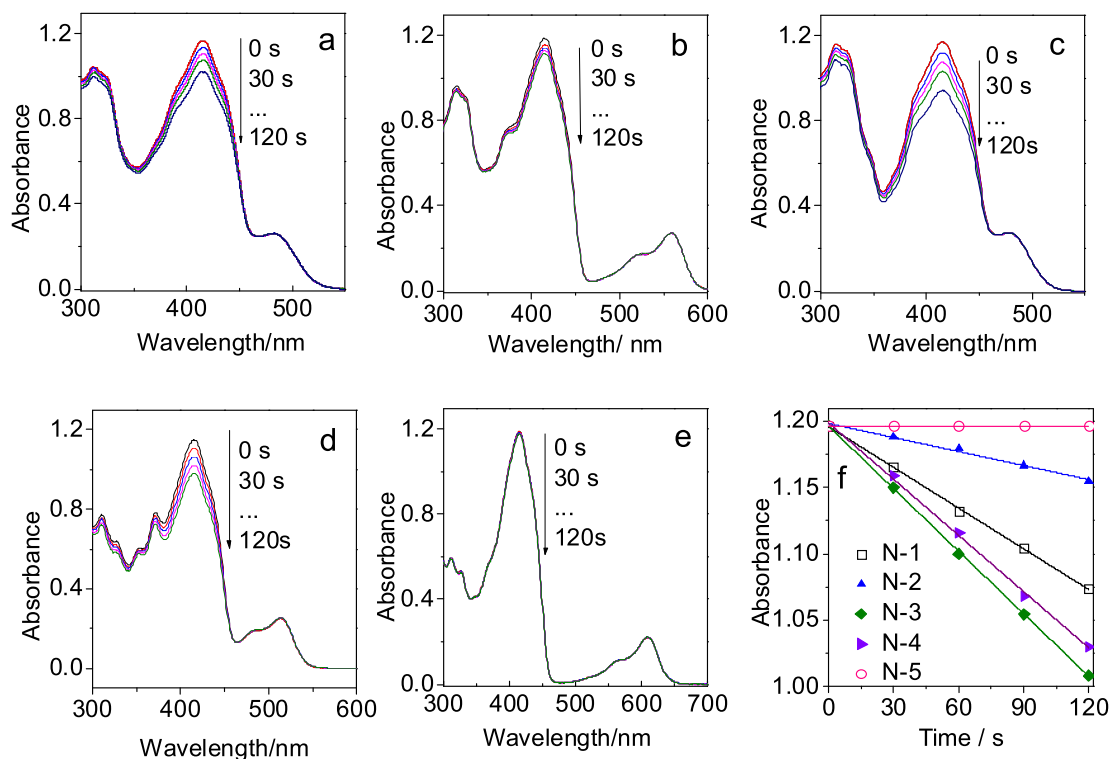


Fig. 5. Absorbance decrease of DPBF at 414 nm with increasing photoirradiation time in the presence of N-1~N-5. (a) N-1, $\lambda_{\text{ex}} = 470$ nm; (b) N-2, $\lambda_{\text{ex}} = 560$ nm; (c) N-3, $\lambda_{\text{ex}} = 470$ nm; (d) N-4, $\lambda_{\text{ex}} = 515$ nm; (e) N-5, $\lambda_{\text{ex}} = 610$ nm; (f) Comparison of photooxidation ability of N-1~N-5 with the same irradiated intensity and the same absorbance of photosensitizers at the irradiation wavelength ($A = 0.20$) in PhCH_3 . Deeper slope indicates more efficient $^1\text{O}_2$ photosensitizing ability, 20°C .

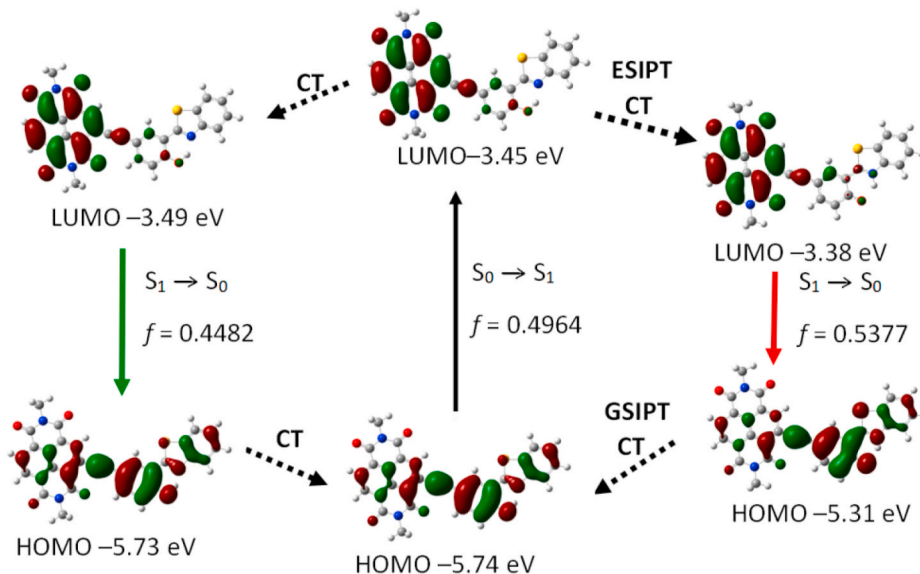


Fig. 6. Selected frontier molecular orbitals involved in the excitation and emission of N-1. Both enol form (left) and cis-keto form (right) were calculated. CT stands for conformation transformation. Toluene was employed as solvent in the calculation. The calculations are at the B3LYP/6-31G(d) level using Gaussian 09W.

611 nm, respectively. They exhibit much longer absorption wavelength in comparison to N-1 and N-2. The red-shifted absorptions of the amino-substituted compounds (N-2, N-4 and N-5) are probably due to the elevated energy level of HOMO orbits, so the energy gap between the HOMO and LUMO orbits become smaller [48]. According to the above results, the UV-vis absorption of the NDI derivatives can be readily adjusted by introduction of the amino substituents on the NDI core.

The fluorescence emission spectra of all the compounds were

studied (Fig. 2). N-1 shows strong fluorescence emission in toluene ($\Phi_{\text{F}} = 68.9\%$) and it is sensitive to the solvent polarity (Fig. 2a). With the increase of solvent polarity, fluorescence intensity of N-1 reduced ($\Phi_{\text{F}} = 9.8\%$ in DCM and 4.4% in THF) (Table 1). Interestingly, dual emission is observed apparently in toluene and CH_2Cl_2 , while it is absent in MeOH and it is sensitive to the solvent polarity [49]. It is roughly concluded ESIPT exists in N-1. The emission band at the shorter wavelength (538 nm) is assigned to the excited enol form, while the longer wavelength at

Table 2

Selected parameters for the vertical excitation (UV–vis absorption and fluorescence emission) of the compounds. Electronic excitation energies (eV) and oscillator strengths (f), configurations of the low-lying excited states of **N-1** and its fluorescent precursors. Calculated by TDDFT//B3LYP/6-31G(d), based on the optimized ground state geometries (PhCH₃ was employed as solvent in all the calculation).

	Electronic transition ^a	Excitation TDDFT/B3LYP/6-31G(d)			
		energy	f^b	Composition ^c	CI ^d
Absorption	$S_0 \rightarrow S_1^e$	2.14 eV (580 nm)	0.4964	H → L	0.7039
	$S_0 \rightarrow S_6$	3.20 eV (388 nm)	0.3143	H–3 → L	0.6927
	$S_0 \rightarrow S_7$	3.34 eV (371 nm)	0.4691	H → L+1	0.6628
Emission (enol)	$S_1 \rightarrow S_0$	1.93 eV (643 nm)	0.4482	H → L	0.7051
Emission (keto)	$S_1 \rightarrow S_0$	1.64 eV (745 nm)	0.5377	H → L	0.7062

^a Only selected excited states were considered. The numbers in parentheses are the excitation energy in wavelength.

^b Oscillator strength.

^c H stands for HOMO and L stands for LUMO. Only the main configurations are presented.

^d Coefficient of the wavefunction for each excitations. The CI coefficients are in absolute values.

Table 3

Selected parameters for the vertical excitation (UV–vis absorption and fluorescence emission) of the compounds. Electronic excitation energies (eV) and oscillator strengths (f), configurations of the low-lying excited states of **N-2** and its fluorescent precursors. Calculated by TDDFT//B3LYP/6-31G(d), based on the optimized ground state geometries (PhCH₃ was employed as solvent in all the calculation).

	Electronic transition ^a	Excitation TDDFT/B3LYP/6-31G(d)			
		energy	f^b	Composition ^c	CI ^d
Absorption	$S_0 \rightarrow S_1^e$	2.15 eV (577 nm)	0.5024	H → L	0.7043
	$S_0 \rightarrow S_5$	3.19 eV (388 nm)	0.2559	H–3 → L	0.3027
				H → L+1	0.6086
Emission (enol)	$S_1 \rightarrow S_0$	1.97 eV (629 nm)	0.4926	H → L	0.7052

^a Only selected excited states were considered. The numbers in parentheses are the excitation energy in wavelength.

^b Oscillator strength.

^c H stands for HOMO and L stands for LUMO. Only the main configurations are presented.

^d Coefficient of the wavefunction for each excitations. The CI coefficients are in absolute values. ^e Both S_1 and S_2 excited states were optimized separately.

682 nm is attributed to cis-keto form. The Stokes shift is up to 144 nm. The cis-keto form emission peak shows drastic red shifts with the increased solvent polarities (eg. 762 nm in CH₂Cl₂) (Fig. 2b) [50]. Dual emission is not observed in CH₃OH and only enol emission with normal Stokes shift of 73 nm was observed. It is reasonable that intramolecular hydrogen bonding (–OH...N–) needed for ESIPT process was prohibited by such solvent [51].

In order to ascertain ESIPT in **N-1**, we prepared the reference compound **N-3** which is very similar to **N-1** except alkylation of –OH. The UV–vis absorption of **N-3** is similar to **N-1** but the fluorescence emission spectrum of **N-3** shows no dual emission. Its emission band is only localized at 500–650 nm in PhCH₃, which is similar to the enol-form emission of **N-1**. Meanwhile, the emission full width at half-maximum (fwhm) of **N-1** is wider than that of **N-3** (calculated by Fig. 2a and c), the existence of dual emissions in **N-1** is also possible [52]. Furthermore, HBT is a well-known ESIPT dyes and we can conclude **N-1** take place

ESIPT based on the above experimental results. The quenching fluorescence of **N-3** in polar solvents is also significant, and no dual emission was observed. It is predictable since ESIPT is completely prohibited by alkylation of –OH in **N-3** [20,21].

N-2 also shows high fluorescence emission in toluene ($\Phi_F = 62.3\%$), but dual emission is not observed due to introduction of electron-donating group (alkylamino group) (Fig. 2b). Alkylamino group increases electron density of NDI, to some extent, affect the strength of H-bonding [49]. That is the main reason for the absence of ESIPT for **N-2**. And another reason is intramolecular charge transfer (ICT) in NDI moiety. The emission intensity of **N-2** is much sensitive to the solvent polarity than **N-1**. Especially in MeOH and CH₃CN, the emission is quenched completely which is also due to ICT.

Although **N-1** and **N-2** have the similar molecular structures, **N-2** does not show ESIPT. It is understandable that NDI is a strong electron acceptor [53]. Once NDI exerts electron-withdrawing function in the excited state, it will decrease O-atom electron density of hydroxyl group which will facilitate proton transfer. Otherwise, alkylamino group in **N-2** compensates the electron loss of NDI in the excited state [35], which is the likely reason for the loss of ESIPT.

Without conjugated connection, the dyads **N-4** and **N-5** show only one emission band at 543 nm and 635 nm in toluene, respectively (Fig. 2d and e). However, no dual emission does not mean no occurrence of ESIPT because it is a ultrafast process. Despite of exciting HBT unit, declining tendency of emissive intensity is observed in **N-4** and **N-5** (Figs. S28d and S28e) but it is difficult to verify whether ESIPT take place or not. It is obviously different from the reported Rhodamine-HBT dyads [22], which shows dual emission (ESIPT).

Comparison with two sorts of molecular structures, N-atoms substituted in the fluorophore maybe result in the lack of ESIPT. The fluorescence quantum yields of **N-4** and **N-5** are 24.3% and 24.2% in weak-polar solvent (Table 1). And they are not very changeable in polar solvent, especially for **N-5**. The photophysical properties of all the compounds in different solvent are summarized in Table 1 and Table S1. Compound **N-3** shows relatively obvious red-shifted emission in polar solvent, which indicates more significant intramolecular charge transfer (ICT) in these compounds.

The excitation spectra at different exciting wavelength were studied electronic coupling of all the compounds (Fig. S28). **N-1** and **N-3** have conjugated structures, when the excitation wavelength is set as 320 nm or 460 nm, the emissive intensity shows minor change. But for the non-conjugated structures such as **N-4** and **N-5** have obviously lower emissive intensity by exciting HBT moiety than the lowest lying absorption band. All the results indicate **N-1** and **N-4** have much stronger electronic coupling than **N-4** and **N-5**. Especially for **N-1**, stronger electronic coupling makes NDI and HBT as a entirety, so the dual emission were observed after exciting HBT (320 nm) and the lowest lying absorption band (460 nm) (Fig. S28a). In addition, to exclude dimeric emission of **N-1**–**N-5**, the emission spectrums were carried out at different concentration (Fig. 3). The linear dependence of emission was observed from very low concentration (2 μmol) to relatively high concentration (10 μmol) and no new emissive band appears. These results mean no dimeric emission exist in these compounds.

The fluorescence excitation spectra of **N-1**–**N-5** were also studied in Fig. S27 [52]. For **N-1**, the excitation spectrum is roughly in accordance with the UV–vis absorption. The excitation spectra of 538 nm (enol form) and 682 nm (cis-keto form) were localized at 300–387 nm and 457–520 nm. Especially, exciting HBT moiety (the region at 300–387 nm) can efficiently produce the emission of 538 nm and 682 nm. The area (457–520 nm) of enol form is a bit weaker than that of cis-keto form. For **N-2**–**N-5**, the similar excitation spectrum were observed.

3.3. Nanosecond time-resolved transient absorption spectra: population of the triplet excited states

Time-resolved spectroscopy was used for study of transient species

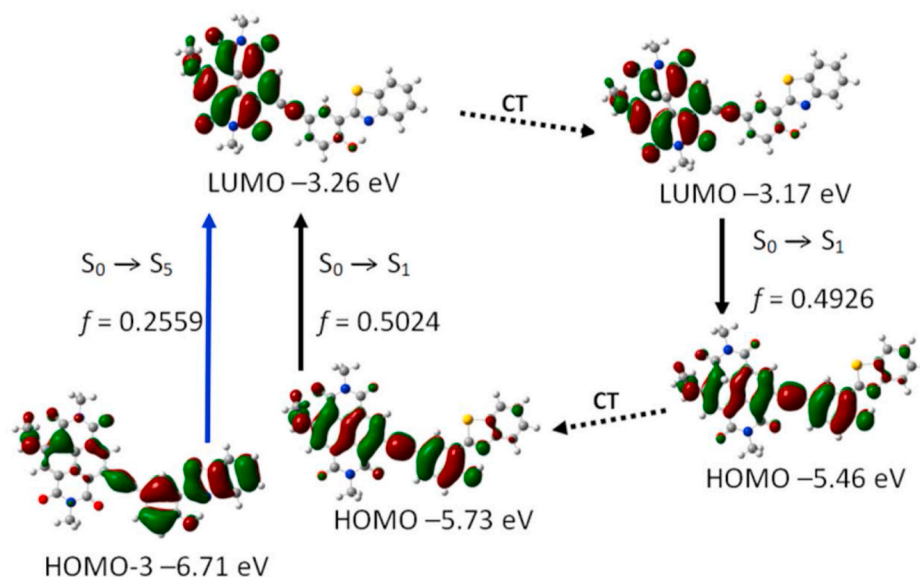


Fig. 7. Selected frontier molecular orbitals involved in the excitation and emission of N-2. CT stands for conformation transformation. Toluene was employed as solvent in the calculation. The calculations are at the B3LYP/6-31G(d) level using Gaussian 09W.

origin from ESIPT dyes, such as triplet excited state and keto-form isomer. Both of them have long-lived lifetime [21,42]. The nanosecond time-resolved transient absorption of N-1~N-5 were carried out (Fig. 4). N-1 shows the weak signal of transient species and the lifetime is 72 μ s in deaerated solution, while it decreases dramatically in presence of oxygen ($\tau_T = 0.59 \mu$ s) (Table 1 and Fig. S29a). This result is absolutely different with the reported compound of NI conjugation with HBT, which shows minor change of lifetime in the presence of oxygen (that is keto tautomer produced by ESIPT) [21]. So it can be concluded the transient species of N-1 is not keto tautomers of ESIPT, but the triplet excited state. For N-2, the long-lived triplet excited state is determined as 121.1 μ s (Fig. S29b).

The stronger signal of triplet excited states were observed in N-3 and N-4. Upon pulsed laser excitation, bleaching band at 480 nm was observed in N-3 and it is in consistent with the UV-vis absorption wavelength. Meanwhile, excited state absorption (ESA) appeared in the range of 350–450 nm and 550–750 nm (Fig. 4a). Triplet state lifetime is determined as 48 μ s (Fig. 4b). N-4 has the longest triplet state lifetime ($\tau_T = 148.5 \mu$ s) (Fig. 4d), which is much longer than the previously observed triplet state lifetime of NDI chromophore (90 μ s) [37]. The ESA appeared at 380–480 nm and 530–700 nm (Fig. 4c), which is the typical triplet state absorption of NDI moiety [35]. NDI moieties in N-3 and N-4 contributed significantly to the T1 excited state, indicated by the bleaching at 480 nm and 515 nm.

3.4. Population and comparison of triplet excited state testified by photooxidation of DPBF

In order to verify the population of triplet excited states, we applied N-1~N-5 to photooxidation of 1, 3-diphenylisobenzofuran (DPBF). It is known that triplet photosensitizers can sensitize O_2 to produce 1O_2 upon photoexcitation. DPBF is employed as the O_2 acceptor (Scheme S1). The production of 1O_2 can be monitored by the absorbance changes at 414 nm. N-1~N-5 have different photooxidation abilities (Fig. 5a~5e). We can observe the absorbance at 414 nm decreased with the extension of irradiation time. The photooxidative effect of N-1~N-5 on the kinetics of 1O_2 production were studied (Fig. 5f). N-1 has less efficient photooxidation ability than N-3 and N-4 showed higher efficiency compare to N-5.

3.5. DFT calculation

DFT/TDDFT calculation has been widely applied to the fluorophores research of the photophysical properties [54–56]. The molecular geometry at the ground state (S_0 state) was optimized by DFT method. UV-vis absorption and the fluorescence emission of the compounds were determined with TDDFT methods.

The optimized ground geometry of N-1 is almost coplanar (Fig. 6). HOMO is distributed on both NDI and HBT moieties, which indicates π -conjugation between two units is obvious. LUMO is almost distributed on NDI moiety, thus the acidity of -OH will increase dramatically upon photoexcitation. It is reasonable that ESIPT will proceed upon photoexcitation subsequently. The calculated excitation energy was 2.14 eV (580 nm). Although the result is lower than the experimental value (2.57 eV, 483 nm), it is not beyond expectation because DFT method always underestimates charge transfer excitation [57,58]. The calculated emission wavelength for enol form is 643 nm (experimental result is 538 nm). No effective transition was found except $S_1 \rightarrow S_0$ transition in the calculation result (Table 2). According to experimental result, the second emissive band at 682 nm has been excluded that exist other lower excited state. And the emission at 682 nm is very likely to be keto-form. The emission peak of cis-keto form is determined at 745 nm (experimental result is 682 nm) and the electron density of cis-keto isomer spread to HBT moiety to some extent, which leads to the stability of cis-keto form in the excited state.

N-2 was calculated with the same methods. The alkylamino group contributes to both HOMO and LUMO orbits, which is the main reason for the red-shifted absorption (compared to N-1). The calculated excited wavelength for $S_0 \rightarrow S_1$ is 577 nm (oscillator strength is 0.5024) and it is very close to the experimental result (560 nm). Another excited wavelength is 388 nm ($S_0 \rightarrow S_5$ transition), which is attributed to the absorption of enol-form of HBT moiety. The calculated emissive band is 629 nm and it is close to the experiment result 582 nm. (Table 3 and Fig. 7).

For N-4, the calculated $S_0 \rightarrow S_1$ transition with oscillator strength of 0.0000, so it is a forbidden transition. It can be regarded as a charge transfer state (dark state). S_2 state is the emissive state and the excited wavelength is 497 nm. It is near to the experimental wavelength (515 nm). The same result is obtained for the emission, that is, the emissive state is S_2 state (oscillator strength is 0.2041). The calculated emission wavelength is 524 nm which is near to the experimental wavelength of 543 nm. HOMO and LUMO are distributed on the HBI and NDI units,

respectively (Table S2 and Fig. S30).

In addition, the calculation of singlet-triplet energy gaps (ΔE_{ST}) can verify separation of the corresponding natural transition orbitals (NTOs) [59]. After optimization of S_1 and T_1 state of partial compounds, ΔE_{ST} of N-1~N-5 are determined to be 1.679 eV, 1.556 eV, 1.699 eV, 1.705 eV and 1.383 eV (Calculated method was shown in ESI). The values is about 1 eV that indicates the sufficient separation of NTOs and make them have the ability of promoting reactive oxygen species (ROS) generation.

4. Conclusions

In summary, the compounds of Naphthalenediimides (NDI) conjugated and non-conjugated with 2-(2-Hydroxyphenyl)Benzothiazole (N-1~N-5) were prepared with the goal to get triplet excited states. The photophysical properties were studied by the steady and transient absorption spectrums. All of them show strong red-shifted absorption compared to HBT. Interestingly, N-1 was obtained as a new ESIPT chromophore, which shows the emission band of the excited enol at 538 nm and cis-keto isomer at 682 nm. Nanosecond time-resolved transient difference absorption spectroscopy demonstrated that triplet state were produced in N-1~N-4 and long-lived triplet excited states (τ_T is up to 148.5 μ s) were populated for the dyes N-4 upon photoexcitation. All the compounds were testified the existence of triplet excited state upon photoexcitation by photooxidation reaction (DPBF). N-3 and N-4 are more effective than others. Our work will supply a new method for the new triplet photosensitizers. It will inspire more work for pursuit of heavy-atom free photosensitizers and the relative research is under way.

Author statement

Jie Ma: Conceptualization, Methodology, Data curation, Writing - Review & Editing, Funding acquisition. **Jinlong Li:** Investigation, Validation. **Rui Yang:** Resources, Investigation. **Weijian Xue:** Visualization, Formal analysis, Funding acquisition. **Qingxia Wang:** Data curation, Formal analysis. **Shenmiao Li:** Supervision, Writing - Original Draft.

Declaration of competing interest

The authors declare that they have no known competing financial interests or personal relationships that could have appeared to influence the work reported in this paper.

Acknowledgements

We thank National Natural Science Foundation (21801146), Natural Science Foundation of Heilongjiang Province (No. QC2016016), University Nursing Program for Young Scholars with Creative Talents in Heilongjiang Province (No. UNPYSCT-2017159), the Fundamental Research Funds in Heilongjiang Provincial Universities (No. 135209304) for financial supports.

Appendix A. Supplementary data

Supplementary data to this article can be found online at <https://doi.org/10.1016/j.dyepig.2021.109225>.

References

- [1] Wu J, Liu W, Ge J, Zhang H, Wang P. New sensing mechanisms for design of fluorescent chemosensors emerging in recent years. *Chem Soc Rev* 2011;40:3483–95.
- [2] Li K, Feng Q, Niu G, Zhang W, Li Y, Kang M, Xu K, He J, Hou H, Tang BZ. Benzothiazole-based AIEgen with tunable excited-state intramolecular proton transfer and restricted intramolecular rotation processes for highly sensitive physiological pH sensing. *ACS Sens* 2018;3:920–8.
- [3] Sedgwick AC, Wu L, Han H, Bull SD, He X, James T, Sessler JL, Tang BZ, Tian H, Yoon J. Excited-state intramolecular proton-transfer (ESIPT) based fluorescence sensors and imaging agents. *Chem Soc Rev* 2018;47:8842–80.
- [4] Sedgwick AC, Dou W, Jiao J, Wu L, Williams GT, Jenkins ATA, Bull SD, Sessler JL, He X, James TD. An ESIPT probe for the ratiometric imaging of peroxyinitrite facilitated by binding to β -Aggregates. *J Am Chem Soc* 2018;140:14267–71.
- [5] Ren H, Huo F, Huang Y, et al. Enhanced SNAR triggered ESIPT to ultrafast NIR fluorescent detection hazardous thiophenols class in environment and living cells. *Dyes Pigments* 2020;181:108567.
- [6] Mutai T, Tomoda H, Ohkawa T, Yabe Y, Araki K. Switching of polymorph-dependent ESIPT luminescence of an imidazo[1,2-a] pyridine derivative. *Angew Chem Int Ed* 2008;47:9522–4.
- [7] Verité PM, Guido CA, Jacquemin D. First-principles investigation of the double ESIPT process in a thiophene-based dye. *Phys Chem Chem Phys* 2019;21:2307–17.
- [8] Kwon JE, Park SY. Advanced organic optoelectronic materials: harnessing excited-state intramolecular proton transfer (ESIPT) process. *Adv Mater* 2011;23:3615–42.
- [9] Chaiwongwattana S, Škalamera D, Došlić N, Bohne C, Basarić N. Substitution pattern on anthrol carbaldehydes: excited state intramolecular proton transfer (ESIPT) with a lack of phototautomer fluorescence. *Phys Chem Chem Phys* 2017;19:28439–49.
- [10] Carayon C, Fery-Forgues S. 2-Phenylbenzoxazole derivatives: a family of robust emitters of solid-state fluorescence. *Photochem Photobiol Sci* 2017;16:1020–35.
- [11] Mutai T, Ohkawa T, Shono H, Araki K. Tuning of excited-state intramolecular proton transfer (ESIPT) fluorescence of imidazo[1,2-a]pyridine in rigid matrices by substitution effect. *J Mater Chem C* 2016;4:3599–606.
- [12] Padalkar VS, Seki S. Excited-state intramolecular proton-transfer (ESIPT)-inspired solid state emitters. *Chem Soc Rev* 2016;45:169–202.
- [13] Suzuki N, Suda K, Yokogawa D, Kitoh-Nishioka H, Irie S, et al. Near infrared two-photon-excited and emissive dyes based on a strapped excited-state intramolecular proton-transfer (ESIPT) scaffold. *Chem Sci* 2018;9:2666–73.
- [14] Wu K, Zhang T, Wang Z, Wang L, Zhan L, Gong S, et al. De novo design of excited-state intramolecular proton transfer emitters via a thermally activated delayed fluorescence channel. *J Am Chem Soc* 2018;140:8877–86.
- [15] Zhao J, Ji S, Chen Y, Guo H, Yang P. Excited state intramolecular proton transfer (ESIPT): from principal photophysics to the development of new chromophores and applications in fluorescent molecular probes and luminescent materials. *Phys Chem Chem Phys* 2012;14:8803–17.
- [16] Grando SR, Pessoa CM, Gallas MR, Costa TMH, Rodembusch FS, Benvenutti EV. Modulation of the ESIPT emission of benzothiazole type dye incorporated in silica-based hybrid materials. *Langmuir* 2009;25:13219–23.
- [17] Luxami V, Kumar S. Molecular half-subtractor based on 3,3'-bis(1H-benzimidazolyl-2-yl)[1,1'] binaphthalenyl -2,2'-diol. *New J Chem* 2008;32:2074–9.
- [18] Nakane Y, Takeda T, Hoshino N, Sakai K, Akutagawa T. ESIPT fluorescent chromism and conformational change of 3-(2-Benzothiazolyl)-4-hydroxybenzenesulfonic acid by amine sorption. *J Phys Chem C* 2018;122:16249–55.
- [19] Ikegami M, Arai TJ. Photoinduced intramolecular hydrogen atom transfer in 2-(2-hydroxyphenyl)benzoxazole and 2-(2-hydroxyphenyl)benzothiazole studied by laser flash photolysis. *J Chem Soc Perkin Trans* 2002;2:1296–301.
- [20] Yang P, Zhao J, Wu W, Yu X, Liu Y. Accessing the long-lived triplet excited states in bodipy-conjugated 2-(2-hydroxyphenyl) benzothiazole/benzoxazoles and applications as organic triplet photosensitizers for photooxidations. *J Org Chem* 2012;77:6166–78.
- [21] Ma J, Zhao J, Yang P, Huang D, Zhang C, Li Q. New excited state intramolecular proton transfer (ESIPT) dyes based on naphthalimide and observation of long-lived triplet excited states. *Chem Commun* 2012;48:9720–2.
- [22] Majumdar P, Zhao J. 2-(2-Hydroxyphenyl)-benzothiazole (HBT)-Rhodamine dyad: acid-switchable absorption and fluorescence of excited-state intramolecular proton transfer (ESIPT). *J Phys Chem B* 2015;119:2384–94.
- [23] Bhosale SV, Bhosale SV, Kalyankar MB, Langford SJ. A core-substituted naphthalene diimide fluoride sensor. *Org Lett* 2009;11:5418–21.
- [24] Bhosale SV, Jani CH, Langford SJ. Chemistry of naphthalene diimides. *Chem Soc Rev* 2008;37:331–42.
- [25] Takenaka S, Yamashita K, Takagi M, Uto Y, Kondo H. DNA sensing on a DNA probe-modified electrode using ferrocenylnaphthalene diimide as the electrochemically active ligand. *Anal Chem* 2000;72:1334–41.
- [26] Lu X, Zhu W, Xie Y, Li X, Gao Y, Li F, et al. Near-IR core-substituted naphthalenediimide fluorescent chemosensors for zinc ions: ligand effects on PET and ICT channels. *Chem Eur J* 2010;16:8355–64.
- [27] Huang Y, Lin Q, Wu J, Fu N. Design and synthesis of a squaraine based near-infrared fluorescent probe for the ratiometric detection of Zn^{2+} ions. *Dyes Pigments* 2013;99:699–704.
- [28] Collie GW, Promontorio R, Hampel SM, Micco M, Neidle S, Parkinson GN. Structural basis for telomeric G-quadruplex targeting by naphthalene diimide ligands. *J Am Chem Soc* 2012;134:2723–31.
- [29] Ajayakumar MR, Asthana D, Mukhopadhyay P. Core-modified naphthalenediimides generate persistent radical anion and cation: new panchromatic NIR probes. *Org Lett* 2012;14:4822–5.
- [30] Au-Yeung HY, Coughon FBL, Otto S, Pantoş GD, Sanders JKM. Exploiting donor-acceptor interactions in aqueous dynamic combinatorial libraries: exploratory studies of simple systems. *Chem Sci* 2010;1:567–74.
- [31] Suraru SL, Würthner F. Regioselectivity in sequential nucleophilic substitution of tetrabromo-naphthalene diimides. *J Org Chem* 2013;78:5227–38.
- [32] Shejul DA, Wagalgave SM, Jadhav RW, Kobaisi MA, La DD, Jones LA, et al. Aggregation-induced emission characteristics and solvent triggered hierarchical

- self-assembled chiral superstructures of naphthalenediimide amphiphiles. *New J Chem* 2020;44:1615–23.
- [33] Sakai N, Mareda J, Vauthey E, Matile S. Core-substituted naphthalenediimides. *Chem Commun* 2010;46:4225–37. <https://pubs.rsc.org/en/content/articlelanding/2010/cc/c0cc00078g>.
- [34] Roux A, Sakai N, Matile S. Amphiphilic dynamic NDI and PDI probes: imaging microdomains in giant unilamellar vesicles. *Org Biomol Chem* 2012;10:6087–93.
- [35] Wu S, Zhong F, Zhao J, Guo S, Yang W, Fyles T. Broadband visible light-harvesting naphthalenediimide (NDI) triad: study of the intra-/intermolecular energy/electron transfer and the triplet excited state. *J Phys Chem A* 2015;119:4787–99.
- [36] Matsunaga Y, Goto K, Kubono K, Sako K, Shinmyozu T. Photoinduced color change and photomechanical effect of naphthalene diimides bearing alkylamine moieties in the solid state. *Chem Eur J* 2014;20:7309–16.
- [37] Liu Y, Wu W, Zhao J, Zhang X, Guo H. Accessing the long-lived near-IR-emissive triplet excited state in naphthalenediimide with light-harvesting diimine platinum (ii) bisacetylido complex and its application for upconversion. *Dalton Trans* 2011;40:9085–9.
- [38] Aveline BM, Matsugo S, Redmond RW. Photochemical mechanisms responsible for the versatile application of naphthalimides and naphthalindiimides in biological systems. *J Am Chem Soc* 1997;119:11785–95.
- [39] Liu L, Guo S, Ma J, Xu K, Zhao J, Zhang T. Broadband visible-light -harvesting *trans*-bis (alkylphosphine) platinum(II)-Alkynyl complexes with singlet energy transfer between BODIPY and naphthalene diimide ligands. *Chem Eur J* 2014;20:14282–95.
- [40] Bhosale SV, Kalyankar MB, Bhosale SV, Langford SJ, Reid EF, Hogan CF. The synthesis of novel core-substituted naphthalene diimides via Suzuki cross-coupling and their properties. *New J Chem* 2009;33:2409–13.
- [41] Park S, Kwon O, Lee Y, Jang D, Park SY. Imidazole-based excited-state intramolecular proton-transfer (ESIPT) materials: observation of thermally activated delayed fluorescence (TDF). *J Phys Chem A* 2007;111:9649–53.
- [42] Iijima T, Momotake A, Shinohara Y, Sato T, Nishimura Y, Arai T. Excited-state intramolecular proton transfer of naphthalene-fused 2-(2'-hydroxyarylyl)benzazole family. *J Phys Chem A* 2010;114:1603–9.
- [43] Yogo T, Urano Y, Ishitsuka Y, Maniwa F, Nagano T. Highly efficient and photostable photosensitizer based on BODIPY chromophore. *J Am Chem Soc* 2005;127:12162–3.
- [44] Wu Y, Zhen Y, Ma Y, Zheng R, Wang Z, Fu H. Crossing in di(perylene bisimide)s: a structural platform toward photosensitizers for singlet oxygen generation. *J Phys Chem Lett* 2010;1:2499–502.
- [45] Adarsh N, Avirah RR, Ramaiah D. Tuning photosensitized singlet oxygen generation efficiency of novel Aza-BODIPY dyes. *Org Lett* 2010;12:5720–3.
- [46] Wang W, Gao Q, Li X, Wang J, Wang C, Zhang Y, Bu X. A water-stable lanthanide-coordination polymer with free Lewis site for fluorescent sensing of Fe³⁺. *Chin Chem Lett* 2019;30:75–8.
- [47] Yia D, Wua Y, Chen C, Wang L, Wang Q, Pu L, Wei S. Preparation of pyrido[1,2-c][1,2,4]triazole-based p-conjugated triazine as a Fe³⁺ ion fluorescent sensor. *Chin Chem Lett* 2019;30:1059–62.
- [48] Guo S, Wu W, Guo H, Zhao J. Room temperature long-lived triplet excited states of naphthalene- diimides and their applications as organic triplet photosensitizers for photooxidation and triplet-triplet annihilation upconversions. *J Org Chem* 2012;77:3933–43.
- [49] Demchenko AP, Tang K, Chou P. Excited-state proton coupled charge transfer modulated by molecular A P structure and media polarization. *Chem Soc Rev* 2013;42:1379–408.
- [50] Hsien C, Jiang C, Chou P. Recent experimental advances on excited-state intramolecular proton coupled electron transfer reaction. *Acc Chem Res* 2010;43:1363–74.
- [51] (a) Chou P, Martinez ML, Clements JH. Reversal of excitation behavior of proton-transfer vs. Charge-transfer by dielectric perturbation of electronic manifolds. *J Phys Chem* 1993;97:2618–22.(b) Seo J, Kim S, Park SY. Strong solvatochromic fluorescence from the intramolecular charge-transfer state created by excited-state intramolecular proton transfer. *J Am Chem Soc* 2004;126:11154–5.
- [52] Chou P, Yu W, Cheng Y, Pu S, Yu Y, Lin Y, Huang C, Chen C. Solvent-polarity tuning excited-state charge coupled proton-transfer reaction in *p*-*N,N*-ditolylaminosalicylaldehydes. *J Phys Chem A* 2004;108:6487–98.
- [53] Kulkarni C, Periyasamy G, Balasubramanian S, George S. Charge-transfer complexation between naphthalene diimides and aromatic solvents. *J Phys Chem Chem Phys* 2014;16:14661–4.
- [54] Zhao G, Liu J, Zhou L, Han K. Site-selective photo induced electron transfer from alcoholic solvents to the chromophore facilitated by hydrogen bonding: a new fluorescence quenching mechanism. *J Phys Chem B* 2007;111:8940–5.
- [55] Zhang X, Wu Y, Ji S, Guo H, Song P, et al. Effect of the electron donor/acceptor orientation on the fluorescence transduction efficiency of the d-PET effect of carbazole-based fluorescent boronic acid sensors. *J Org Chem* 2010;75:2578–88.
- [56] Shao J, Guo H, Ji S, Zhao J. Styryl-BODIPY based red-emitting fluorescent OFF–ON molecular probe for specific detection of cysteine. *Biosens Bioelectron* 2011;26:3012–7.
- [57] Dreuw A, Weisman JL, Head-Gordon M. Long-range charge-transfer excited states in time-dependent density functional theory require non-local exchange. *J Chem Phys* 2003;119:2943–6.
- [58] Kowalczyk T, Lin ZL, Voorhis TV. Fluorescence quenching by photoinduced electron transfer in the Zn²⁺ sensor zinpyr-1: a computational investigation. *J Phys Chem A* 2010;114:10427–34.
- [59] Xu W, Lee MMS, Nie J, Kwok RTK, Lam JWY, Xu F, Wang D, Tang BZ. Three-pronged attack by homologous far-red/NIR AIEgens to Achieve 1+1+1>3 synergistic enhanced photodynamic therapy. *Angew Chem Int Ed* 2020;59:9610–6.